Geophys. J. Int. (2004) **157,** 1119–1129 doi: 10.1111/j.1365-246X.2004.02294.x

Paramagnetic and ferromagnetic anisotropy of magnetic susceptibility in migmatites: measurements in high and low fields and kinematic implications

Eric C. Ferré,[1] Fátima Martín-Hernández,[2] Christian Teyssier[3] and Mike Jackson[4]

[1]*Department of Geology, Southern Illinois University, Carbondale, IL* 62901, *USA. E-mail: eferre@geo.siu.edu*
[2]*Paleomagnetic Laboratory 'Fort Hoofddijk', Utrecht University,* 3584 *CD Utrecht, The Netherlands*
[3]*Department of Geology and Geophysics, University of Minnesota, Minneapolis, MN* 55455, *USA*
[4]*Institute for Rock Magnetism, University of Minnesota, Minneapolis, MN* 55455, *USA*

Accepted 2004 February 27. Received 2004 February 13; in original form 2003 May 16

SUMMARY

The separation of paramagnetic and ferromagnetic anisotropy of magnetic susceptibility (AMS) is achieved in this study by using a vibrating sample magnetometer and a torque magnetometer performing directional anisotropy measurements in sufficiently high fields to saturate the ferromagnetic phases. The studied material, a migmatite from Minnesota, has a magnetic mineralogy characterized by ferrimagnetic multidomain titanomagnetite, paramagnetic biotite and a diamagnetic quartzo-feldspathic matrix. The low-field AMS represents the sum of ferromagnetic and paramagnetic contributions because the quartz contribution can be neglected, its magnetic susceptibility being two orders of magnitude smaller than that of biotite. In contrast, measurements in a high field isolate the paramagnetic component of the magnetic fabric. The high-field AMS is consistent between specimens and correlates well with measurements done using the torque magnetometer. The magnetic fabrics of the ferromagnetic and of the paramagnetic minerals are not co-axial, i.e. the subfabrics of the biotite and the magnetite are distinct. We propose that this non-coaxiality is due to a vorticity component during regional deformation and that it reflects the general conditions of deep crustal orogenic deformation.

Key words: AMS, high-field, magnetic anisotropy, migmatite, paramagnetism.

1 INTRODUCTION

Magnetic fabrics have long been considered as proxies for mineral fabrics in a wide range of materials (Hrouda 1982; Rochette *et al.* 1992; Tarling & Hrouda 1993; Borradaile & Henry 1997). The success of magnetic fabric methods lies in their ability to measure the orientation of hundreds of grains within minutes, as opposed to the universal stage or electron backscattered diffraction methods (≈8 hours/sample). The anisotropy of magnetic susceptibility (AMS) measured in low field has proved to be particularly useful for studying the flow of igneous rocks, both volcanic and plutonic (e.g. Cañón-Tapia *et al.* 1996; Bouchez 1997). A recent study showed that this method could be a valuable tool for studying the petrofabric of migmatites (Ferré *et al.* 2003). In these migmatites, the low-field AMS fabric is largely dominated by the shape anisotropy of primary multidomain magnetite, a strongly ferrimagnetic phase, that masks the contribution of biotite.

The kinematic significance of AMS fabrics might be questioned because ferromagnetic phases, which dominate magnetic properties in low field, generally account for only a minor volume of the rocks (<1 per cent). In addition, the fabric of ferromagnetic minerals is not necessarily the same as that of paramagnetic minerals because the two types of magnetic mineral might have formed at different stages and might have undergone distinct deformation paths.

Hence, various experimental approaches have been used to try and separate the paramagnetic and ferromagnetic components of the AMS fabric. Henry (1983) proposed a statistical method based on the analysis of several specimens from the same site for discrimination between paramagnetic and ferromagnetic subfabrics. Rochette & Fillion (1988) used a cryogenic high-field magnetometer. Hrouda & Jelinek (1990) proposed a mathematical method to separate the components based on measurements at different fields with a high-field torque magnetometer. Jackson (1991) used the anisotropy of remanent magnetization for the discrimination. This method was refined by Hrouda (2002) using the normalization method of Jelínek (1993) for multidomain magnetite. Richter *et al.* (1993) and Parès & van der Pluijm (2003) successfully used the variation of susceptibility of paramagnetic minerals at low temperature to isolate their anisotropy. Here we present several significant improvements to the separation method based on high-field measurements with a vibrating sample magnetometer (VSM) that was initially proposed by Thill *et al.* (2000), Ferré *et al.* (2000) and Kelso *et al.* (2002). Our new method is tested against the well-established torque

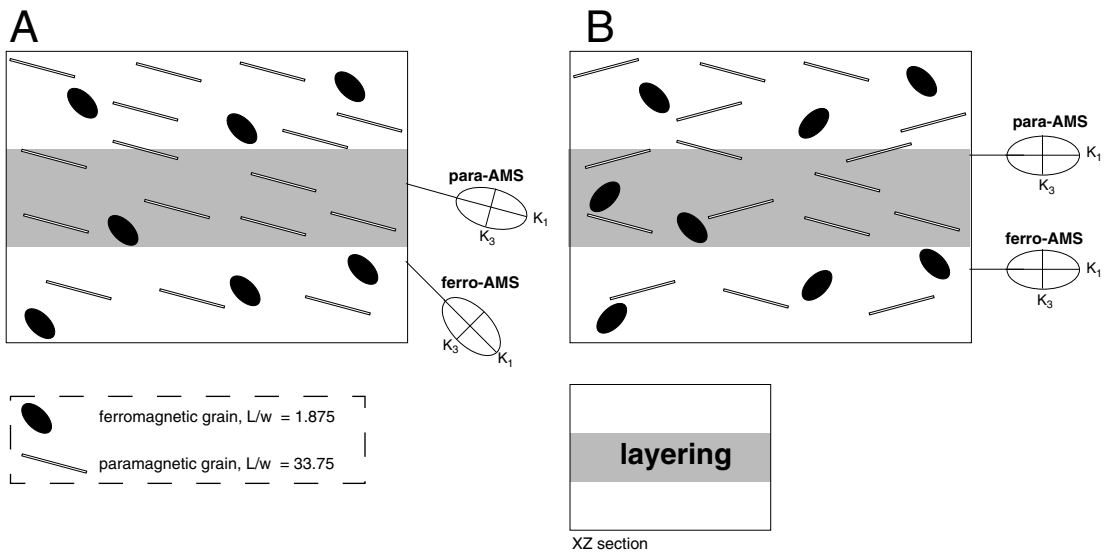

Figure 1. *XZ* section models presenting different possible configurations for paramagnetic and ferromagnetic AMS fabrics.

magnetometry method (Banerjee & Stacey 1967; Collinson *et al.* 1967; Hrouda & Jelinek 1990; Martín-Hernández & Hirt 2001).

The materials chosen for our investigations are migmatites on which extensive low-field magnetic studies have already been performed (Ferré *et al.* 2003). Migmatites represent typical continental lower crust material and potentially hold important information on deep crustal flow under partial melting conditions. These heterogeneous rocks result from crustal melting, typically at depths greater than 15 km and at temperatures exceeding 650 °C (e.g. Zen 1988). The structural analysis of migmatites is complicated by the fact that during metamorphism they behave in part like solids and in part like granitic liquids (McLellan 1983; Passchier *et al.* 1990; Vigneresse *et al.* 1996; Hopgood 1998). The viscosity contrast between the leucosome and the melanosome often results in the development of complex folds (recumbent, contorted and sheath folds) at the scale of a few centimetres to a few metres. The structural complexity masks an intrinsic fabric homogeneity that results from crystal plastic flow and recrystallization at high temperature.

In the studied migmatites, both the ferromagnetic and paramagnetic minerals are primary and are thought to have been deformed simultaneously. The magnetocrystalline anisotropy carried by paramagnetic carriers results from the intrinsic anisotropy of individual grains and their lattice-preferred orientation (LPO). In contrast, the ferromagnetic anisotropy results mainly from the magnetostatic anisotropy of magnetite. Our objective is to separate the paramagnetic AMS from the low-field, ferromagnetic-dominated AMS. Differences between these two kinds of AMS might result from the carriers having distinct intrinsic anisotropies and/or non-coaxial deformation affecting particles with different aspect ratios. Fig. 1 shows theoretical configurations in which the ferromagnetic AMS and the paramagnetic AMS are either non-coaxial (A) or coaxial (B). Configuration A may arise in a simple shear regime whereas configuration B would occur in a pure shear regime. The separation of the bulk AMS into subfabrics has the potential to provide important constraints on flow regime and vorticity in the lower continental crust during orogenic processes.

2 REGIONAL SETTING, ROCK TYPES AND STRUCTURES

Previous studies have detailed the regional setting, lithological types and structures of the studied migmatites (Bauer 1974, 1980; Goldich *et al.* 1980; Nielsen & Weiblen 1980; Southwick & Chandler 1996). The following is only a summary of key features.

The study area is part of the Minnesota River Valley Complex in the Superior Province of the Canadian Shield. The region has been subdivided into several Archean crustal blocks separated by east–west north-dipping shear zones. The sampling area is located near the town of Morton which hosts several small quarries and glacier-polished outcrops. Late Cretaceous sedimentary rocks and Quaternary glacial deposits cover the rest of the area.

The main lithological types are essentially amphibolite- to granulite-grade gneisses with tonalitic, granodioritic, dioritic and pelitic types, interlayered and grading into each other (>3.0 Ga). The gneisses consist mostly of quartz, alkali feldspar, plagioclase, biotite and hornblende while the dominant opaque minerals are magnetite and ilmenite. The magnetite grains are fairly large (20 to 200 μm), euhedral, elongate and widely separated from each other. The number of grains per 25 mm diameter thin section is generally less than 10. The main rock types are coarse-grained quartzo-feldspathic migmatite, amphibolite and minor granite. The prominent layering is formed by alternating layers of pink alkali feldspar-rich granitic leucosome, grey plagioclase-rich tonalitic leucosome and dark mafic melanosome at a scale of a few millimetres to a few centimetres (Fig. 2). The pink colour of the granitic leucosome is pervasive at the scale of the sampling area. Amphibolites form distinctive boudinaged layers (up to 3 m thick) or inclusion trails and are always surrounded by the tonalitic leucosome. This grey leucosome is commonly spotted by amphibole clots of about 1 cm in diameter. Dykes and veins of microgranite, aplite and pegmatite, a few centimetres in width, sharply cut through the migmatites. Amphibolite inclusions range in shape from small rounded inclusions of a few tens of centimetres in diameter to large boudins of a few tens of metres in length and up to 3 m in width. Five distinct layers of

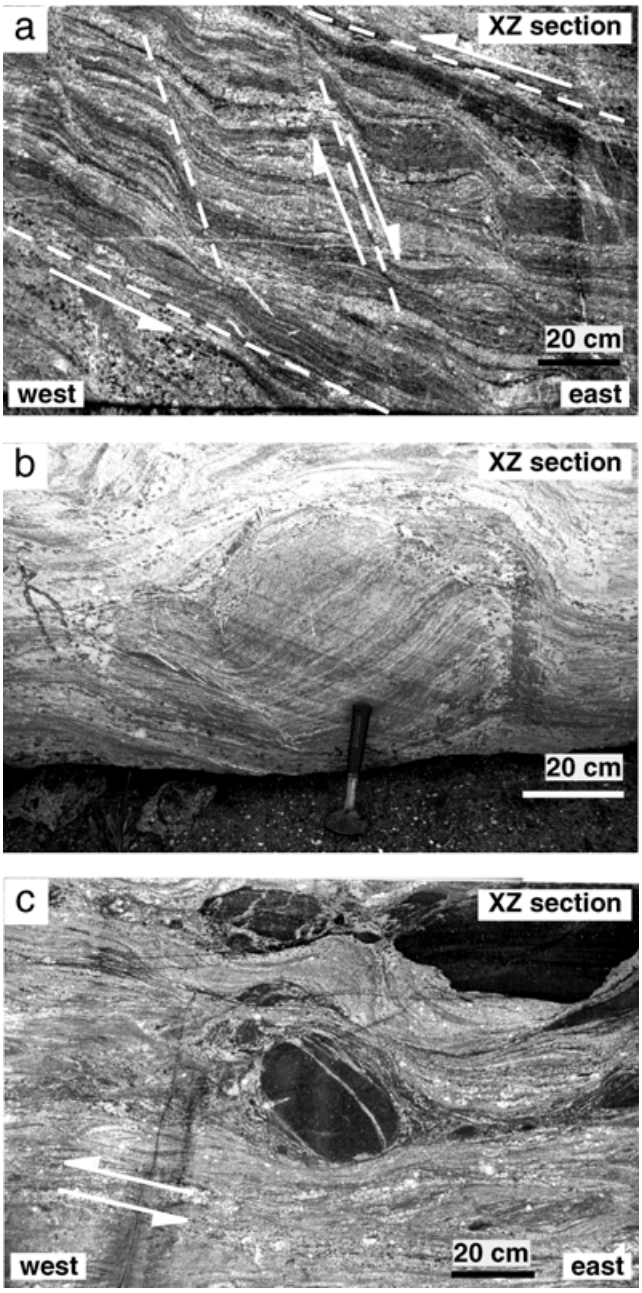

Figure 2. Field structures of the Morton migmatites with evidence for non-coaxial deformation. All photographs are in the *XZ* plane of the finite strain ellipsoid. See Ferré *et al.* (2003) for details.

amphibolite inclusions outcrop in one of the quarries, over a height of about 30 m, strike north–south and dip 10 to 20° to the east. These inclusions display small-scale structures such as cracks and sharp edges resulting from brittle behaviour during partial melting and regional deformation.

At the outcrop scale, the most prominent structure is a compositional layering which gently dips 20° to the east with nearly parallel foliation (Fig. 2). A few mineral stretching lineations and mineral aggregate lineations, observed in quartz-rich layers from weathered outcrops, are subhorizontal and trending around 075°N. The quarry walls are wire-cut almost parallel to the principal planes of geological strain while the floor is close to the layering plane. A few amphibolite layers, a few tens of centimetres in thickness, occur as refractory boudins subparallel to the migmatite layering and are interpreted as former tholeiitic basalt sills or dykes. Regional deformation was coeval with pervasive partial melting which resulted in the formation of different leucosomes derived from different protoliths. Large-scale open upright folds have an average wavelength of 10 km and fold axes trending 080–090°N and plunging 10°E. The layered migmatites systematically display shear bands and back-rotated blocks of slightly different composition which, when observed in sections perpendicular to the foliation and parallel to the layering, indicate a consistent top-to-west sense of shear. The zones displaying back-rotated blocks form corridors of about 1 m in thickness immediately bounded by biotite-rich zones. At the regional scale, folding seems to post-date the development of the foliation (Bauer 1974). The migmatites are cut by late-kinematic to post-kinematic granitoid intrusions (≈2.6 Ga). Finally, some of the north-dipping shear zones were probably reactivated under lower-grade metamorphic conditions during the Penokean orogeny (2.45–1.75 Ga).

3 PRINCIPLES AND METHODS OF MAGNETIC ANISOTROPY MEASUREMENTS

3.1 General principles of AMS measurements and sampling procedure

The magnetic susceptibility, K, is defined by the ratio between the induced magnetization of the specimen and the inducing magnetic field. This magnetization disappears when the field is relaxed. The anisotropy of magnetic susceptibility is described by a symmetric second-rank tensor with three principal axes ($K_1 \geq K_2 \geq K_3$). K_1 is the magnetic lineation and K_3 is normal to the magnetic foliation. The bulk magnetic susceptibility, K_m, is the arithmetic mean of the principal susceptibilities [$K_m = 1/3\,(K_1 + K_2 + K_3)$]. The degree of anisotropy is given by P_j where

$$P_j = \exp\left(\sqrt{2[(\eta_1 - \eta)^2 + (\eta_2 - \eta)^2 + (\eta_3 - \eta)^2]}\right)$$

with

$$\eta = \frac{\eta_1 + \eta_2 + \eta_3}{3}.$$

The ellipsoid shape is characterized by the parameter T (Jelínek 1978).

$$T = [2(\eta_2 - \eta_3)/(\eta_1 - \eta_3)] - 1 \quad \text{with} \quad \eta_i = \ln K_i.$$

Problems associated with weathering are insignificant because samples were collected from recent quarries. Sixty oriented cores were drilled from five stations. Each core was 25 mm in diameter and long enough to make at least three specimens which yielded a total of 217 core specimens. These cores were cut at a length of 22 mm to conform to the cylinder length/diameter ratio of 0.85 of Noltimier (1971). For the high-field study, 36 cube specimens of 20 ± 0.5 mm length were cut from a large oriented block.

3.2 Measurement of low-field anisotropy of magnetic susceptibility with a Kappabridge susceptometer

The measurements of magnetic susceptibility and AMS were carried out using a low alternating inductive magnetic field ($\pm 4 \times 10^{-4}$ T, 920 Hz) on a Kappabridge KLY-2 susceptometer (Agico, Brno). Each specimen was measured in 15 different positions to calculate the anisotropy magnitude and orientation of the magnetic

susceptibility ellipsoid (Jelínek 1977). Temperature variation of the sample during the 5-min AMS measurement is estimated to be <1 K causing an error in the anisotropy of less than 0.3 per cent.

In order to identify different ferromagnetic contributions thermomagnetic experiments were performed in low field under Ar flux with a CS-2 furnace attached to the KLY-2 susceptometer. Samples were fragments obtained from 17 rock specimens.

3.3 Measurement of high-field anisotropy of magnetic susceptibility with a vibrating sample magnetometer

The general methodology for measurement of the high-field anisotropy of magnetic susceptibility (HFAMS) using a vibrating sample magnetometer has been described by Thill *et al.* (2000), Ferré *et al.* (2000) and Kelso *et al.* (2002). We present in the following a series of substantial improvements to the original methodology. The HFAMS was determined on the same cubic specimens that were used for the low-field measurements. A series of hysteresis curves were acquired in different orientations for each specimen (Fig. 3), using a vibrating sample magnetometer (Princeton Measurements model 3900). Specimens were left lying on the VSM bench for at least 30 min before measurement to ensure thermal equilibrium with the pole gap space (19 °C) which is cooler than room temperature (21 °C). The same sample holder is used for the directional measurements of the cubic specimens. The magnetic contribution of the sample holder was systematically subtracted in high-field calculations. In contrast with the set-up described in Kelso *et al.* (2002), the bottom of the specimen holder was left free to avoid complications due to erratic friction during rotation. The specimen remains centred in the field within 0.5 mm thanks to a rigid holding rod.

Out of 36 specimens, only 15 were close enough to a perfect cubic shape of $20 \times 20 \times 20 \pm 0.5$ mm to be analysed (Fig. 4). The multiple positions were achieved by eight rotation increments of 45° about the three perpendicular axes perpendicular to faces (X, Y and Z; Fig. 3). Rotations were clockwise as viewed from the top. This yielded 24 hysteresis curves per specimen. Symmetrical positions within the HFAMS measurement scheme are used to estimate the

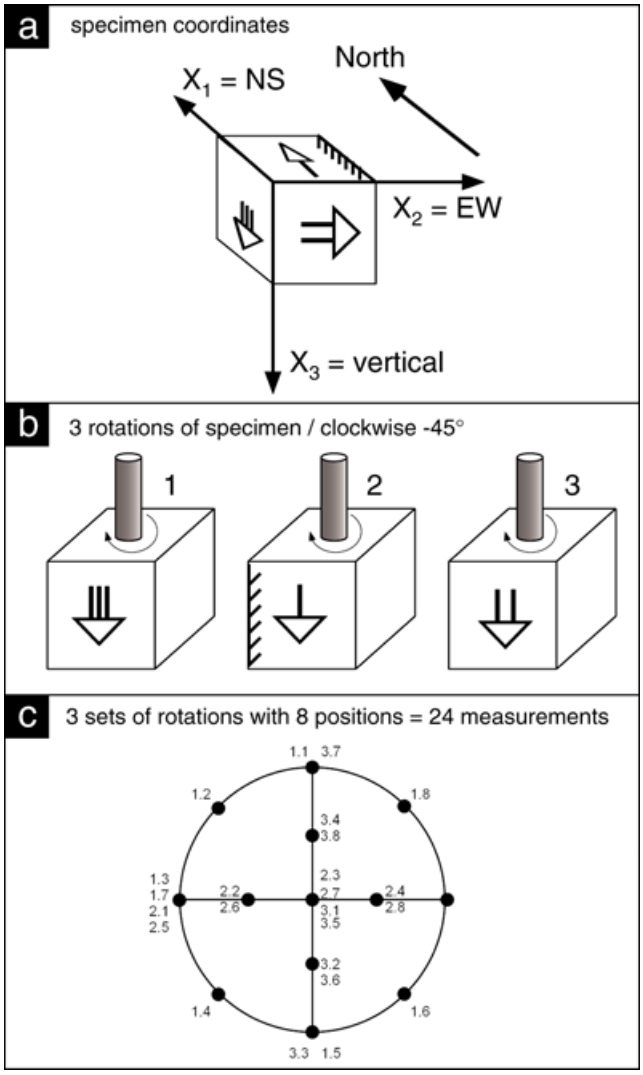

Figure 3. Specimen coordinates, measurement scheme and orientations for the high-field measurements on the vibrating sample magnetometer.

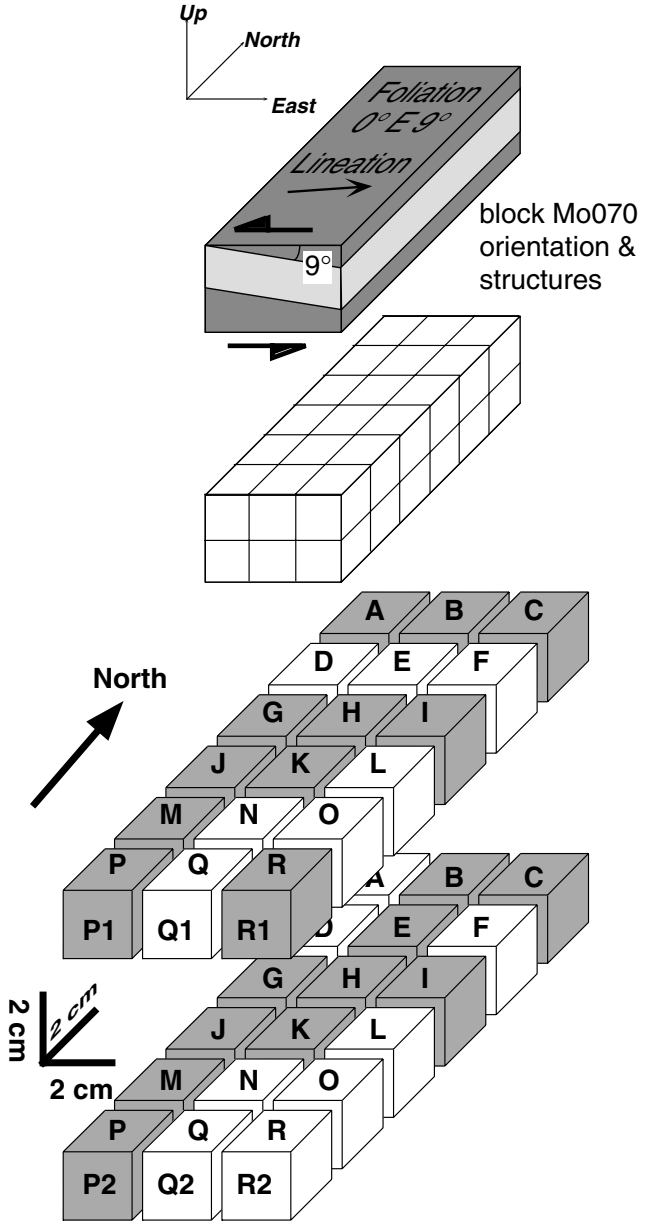

Figure 4. Position and numbers of analysed specimens with respect to mesoscopic structures on oriented block Mo070.

analytical error. Space for the specimen was provided by moving the pole pieces further apart (50 mm) which reduces the maximum field intensity to about 900 mT. The total measurement time per sample was approximately 22 min.

The calculation of the high-field magnetic susceptibility is based on the measurement of the high-field slope (χ_{HF}) of the hysteresis curve. This is done by using the highest 15 per cent of the field range (>765 mT), where the ferromagnetic component is saturated and therefore contributes nothing to the slope. The saturation conditions will be discussed further in the text. Instrument artefacts, such as hooks on the terminations of hysteresis curves related to pole-piece saturation, were removed before calculation. The linear correlation coefficient was better than 0.9999 in all cases which shows that the considered segments were above magnetic saturation.

The response of the VSM instrument depends on the position of the magnetic dipoles with respect to the pick-up coils, and the measured values are therefore sensitive to the shape of the specimen. The advantage of using cubic specimens is clear when considering that such specimens produce an unambiguous geometric/instrument response effect characterized by a 4ω periodicity, and that the instrument response is the same for all three axes, which is not the case with cylindrical specimens. This approach corrects for most variations due to the instrument response of the VSM but not for the fact that the magnetic centre of the specimen (determined by optimizing the position of the specimen in between the coils) does not necessarily coincide with the geometric centre of the specimen. This is the case when magnetic grains are non-uniformly distributed in the specimen. In addition to previous corrections, the high-field slope is finally normalized by dividing χ_{HF} by M_s, the saturation magnetization. M_s can be assumed to be a constant (i.e. independent of measurement direction) for each specimen, and the normalization thus compensates for angular variations due to the shape of the sample and the instrument response function. The residual error after normalization to M_s is on average around 1 per cent, whereas it was around 2.5 per cent before normalization.

3.4 Measurement of high-field anisotropy of magnetic susceptibility with a torque magnetometer

Cubic specimens of length 20 mm were measured in the high-field torque magnetometer at ETH-Zurich (Bergmüller *et al.* 1994). The sample temperature in the torsion instrument was 20 ± 0.5°C. Specimens were measured using four magnetizing fields (1.2, 1.4, 1.6 and 1.8 T) high enough to saturate the ferrimagnetic contribution to the anisotropy. Processing the torque signal measured after rotating the sample by 360° in three perpendicular planes allows for the separation of the paramagnetic and ferrimagnetic contribution to the magnetic anisotropy (Martín-Hernández & Hirt 2001). For each specimen the dependence of the torque amplitude on the square of applied field was tested in order to exclude the presence of haematite. Haematite would contribute to the torque signal as a function of the applied field (Porath & Chamalaun 1966). The measurements take approximately 6 h per sample for a series of four fields. The torque magnetometer, with an interpole space of about 100 mm, provides a homogeneous field (±5 mT) within a much larger volume than the VSM instrument. More importantly, the measured torque does not depend on the position of a magnetic dipole within the uniform field. Consequently, shape effects are practically insignificant. However, the torque magnetometer provides only deviatoric values of the susceptibility tensor because the torque signal is related to the differences in magnetic susceptibility semi-axis (Banerjee & Stacey 1967; Collinson *et al.* 1967; Martín-Hernández & Hirt 2001). An additional measurement of the high-field paramagnetic bulk susceptibility is required in order to compute the full paramagnetic tensor. The shape ellipsoid is defined by the U parameter (Jelínek 1981), $U > 0$ for oblate ellipsoids and $U < 0$ for prolate ellipsoids.

4 LOW-FIELD MAGNETIC DATA

The following is a summary of previous results (Ferré *et al.* 2003). A total of 217 specimens including 36 cubes (20 mm) were measured and the main results are plotted in Fig. 5. Representative measurements are given in Table 1. Thermomagnetic experiments conducted on a few tens of crushed specimens consistently show a significant decrease in magnetic susceptibility between 526 and 548 °C which, in agreement with petrographic observations and electron microprobe data, indicates the presence of titanomagnetite ($X_{ulv} \approx 6$ to 8 per cent). No significant decrease of magnetic susceptibility was observed between 600 and 680 °C. Most of the experiments were not reversible which suggests that thermally induced reactions occurred.

In the 36 cube specimens used for high-field AMS study the magnetic susceptibility ranges from 800 to 27 000 μSI with an average of 6700 ± 5700 μSI. The large variability of K_m at the scale of a few centimetres suggests that the distribution of magnetite grains is heterogeneous at that scale. The degree of anisotropy, P_j, is high and ranges from 1.17 to 1.33 with an average of 1.24 ± 0.04. The degree of magnetic susceptibility anisotropy does not correlate with K_m. The shape of the AMS ellipsoids is described by the T parameter of Jelínek (1978) and is dominantly prolate.

A stereonet of low-field AMS data is presented for cubic specimens from block Mo070 (Figs 6a and b). Maps of magnetic lineations and the trace of the foliation are reported in Fig. 6(c). Low-field magnetic fabrics are homogeneous at the scale of a few centimetres. The eigenvector of the magnetic lineation is 090°, 19° and that of the magnetic foliation is 320°, 67°.

5 HIGH-FIELD MAGNETIC DATA

5.1 High-field vibrating sample magnetometer data

A preliminary study of hysteresis properties was carried out on small rock fragments (≈200 mg) and on separated biotite grains. The fragments contain a ferromagnetic phase identified as titanomagnetite using thermomagnetic methods. The hysteresis properties, plotted in the Day diagram (Day *et al.* 1977), are consistent with multidomain (MD) to pseudo-single domain (PSD) titanomagnetite (Ferré *et al.* 2003). The separated biotites display a purely paramagnetic behaviour suggesting the absence of magnetite microinclusions which may have complicated the interpretation of magnetic fabrics.

This study is based on 1288 hysteresis loops measured on 15 oriented cube specimens (20 mm) at 19 °C. For each cube, a series of 24 (or 48) hysteresis loops were measured at different orientations for rotation increments of 45° (or 22.5°) along three perpendicular axes. Rotation increments of 10° and data reproducibility tests were satisfactorily conducted on several specimens.

The saturation magnetization (M_s) is reached when the second derivative of the induced magnetization M with respect to the magnetizing field B (d^2M/dB^2) tends toward zero. This condition was considered satisfied for the part of the hysteresis loop corresponding to $|d^2M/dB^2| < 10^{-12}$ A m^2 T^{-2}. Ferromagnetic saturation was reached below 400 mT for all specimens. The last five points of each branch of the hysteresis loop, for which pole-piece saturation

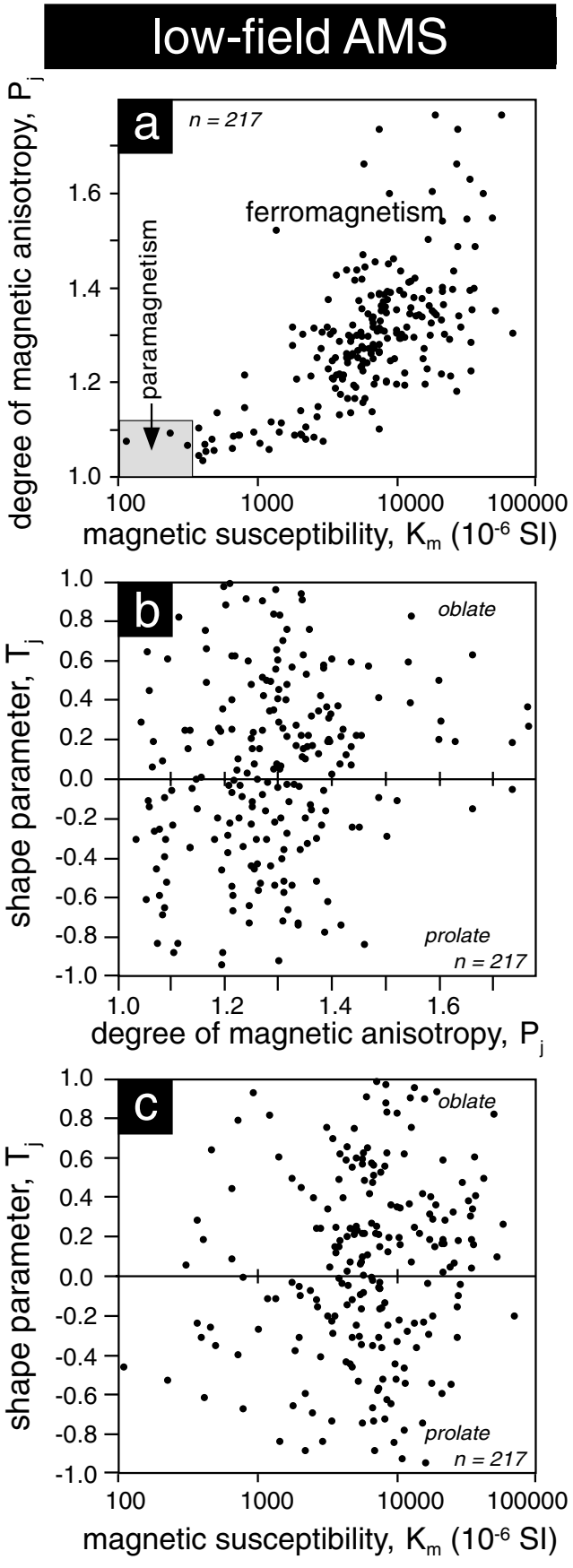

Figure 5. Low-field AMS scalar results on migmatite samples from the study area (Ferré *et al.* 2003).

Table 1. Low-field and high-field magnetic susceptibility data.

	Low-field AMS Kappabridge measurements (10^{-6} SI dimensionless)			High-field AMS VSM measurements (10^{-6} SI dimensionless)		
Specimen	*K*	*P*	*T*	*K*	*P*	*T*
H1	5474	1.304	0.067	139	1.155	0.547
I1	6569	1.329	0.272	250	1.171	0.217
J1	5447	1.232	−0.086	193	1.077	0.500
J2	7365	1.248	−0.563	127	1.127	0.841
K1	5564	1.275	−0.159	128	1.121	0.670
M1	4346	1.250	−0.138	105	1.054	0.568
M2	2522	1.304	0.401	82	1.149	0.338
P1	1882	1.201	−0.370	80	1.014	0.313
R1	4017	1.207	−0.029	72	1.044	−0.297
Average	4798	1.261	−0.067	131	1.101	0.411
S.D.	1792	0.045	0.297	58	0.056	0.327
Max.	7365	1.329	0.401	250	1.171	0.841
Min.	1882	1.201	−0.563	72	1.014	−0.297

generated spurious data, were discarded. M_s is an isotropic property for magnetite and should not vary with specimen orientation. The variability of the measured saturation magnetization for different orientations of the specimen results from non-uniform instrument response when the position of the specimen changes within the field. The M_s of each specimen shows a positive linear correlation ($r^2 = 0.995$) with the low-field bulk magnetic susceptibility K_m of the same specimen. The average M_s (15 specimens) is 0.27 ± 0.09 A m^2 kg^{-1} with a range from 0.10 to 0.40 A m^2 kg^{-1} due to various concentrations of titanomagnetite.

The high-field magnetic susceptibility (χ_{HF}) is measured above 765 mT, well above the saturating field for the ferromagnets in these specimens. χ_{HF} ranges from 71 to 193 μSI with an average of 111 ± 36 μSI (Table 1 and Fig. 7a). The degree of magnetic anisotropy, P_{HF} ranges from 1.01 to 1.24 with an average of 1.12 ± 0.07 (Fig. 7b). The shape parameter, T_{HF} varies from −0.30 to 0.84 with an average of 0.38 ± 0.27 (Fig. 7c). The high-field AMS ellipsoids are oblate (with the exception of one specimen).

Two stereonets of high-field AMS data are presented for 15 cubic specimens from block Mo070 (Fig. 8). The eigenvector of the magnetic lineation is 076°, 23° and that of the magnetic foliation is 343°, 77°.

5.2 High-field torque magnetometer data

Before performing our torque measurements, the low-field AMS of three selected specimens was remeasured on another Kappabridge KLY-2 instrument at ETH-Zurich. The two sets of low-field measurements are perfectly identical, which demonstrates that the VSM measurements did not alter the original magnetic anisotropy. The torque measurements show that ferromagnetic minerals account for 87 per cent of the magnetic susceptibility anisotropy while paramagnetic minerals represent only 13 per cent. The square of the applied field plotted against the maximum torque displays a set of linear regressions for three orientations of the specimens which proves that saturation was achieved in the experiments (Fig. 9a). The paramagnetic shape parameters correspond to oblate ellipsoids ($U \approx 0.23$) whereas the ferromagnetic demagnetization ellipsoids are slightly prolate ($U \approx -0.11$). There is good interspecimen consistency in principal directions for both the paramagnetic and the ferromagnetic torque components (Figs 9b and c). The paramagnetic torque axes depart significantly from the low-field AMS axes and from the principal axes of the ferromagnetic demagnetization ellipsoid.

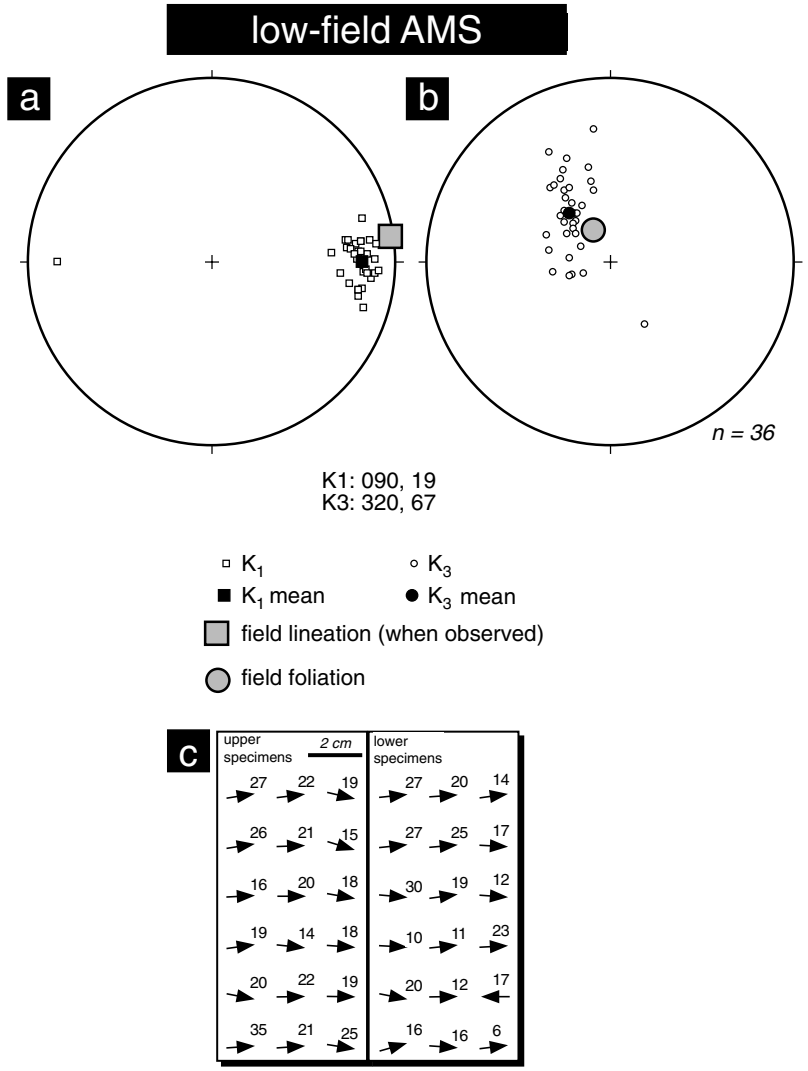

Figure 6. Low-field AMS directional results on oriented block Mo070 used for the high-field study.

6 DISCUSSION

6.1 Significance of low-field magnetic fabrics

The large magnitude of the low-field magnetic susceptibility K_m and of the degree of anisotropy P_j suggests that the low-field AMS is dominated by a ferromagnetic phase. Further investigation with thermomagnetic experiments indicates that titanomagnetite is present in large quantities. The hysteresis properties of this titanomagnetite are consistent with a MD to PSD magnetic granulometry. The excellent positive correlation between K_m and M_s($r^2 = 0.995$) suggests that no other ferromagnetic phases significantly contribute to the low- or high-field properties. It should also be noted that the variability of K_m and M_s over the series of cubic samples used for the high-field study are comparable. This further supports the idea that the hysteresis properties are controlled by the same ferromagnetic phase that dominates the low-field magnetic properties, i.e. titanomagnetite. Previous work has shown that the shape anisotropy of this titanomagnetite had probably been acquired through crystal plastic deformation processes at high temperature and was therefore representative of the high-grade flow of these migmatites (Ferré *et al.* 2003). The low-field AMS fabric can be used as a proxy for finite strain principal axes.

6.2 Significance of high-field magnetic fabrics

The intensity of the magnetizing field in our measurements was 0.9 T. Hrouda & Jelinek (1985) and Rochette & Fillion (1988) have suggested that such a field might be insufficient to saturate minerals with high coercivity and that even 0.8 T might not be enough to saturate magnetite. Our measurements, on the contrary, show satisfactory saturation conditions. This is further supported by the remarkable consistency of high-field fabrics. The high-field slope, calculated above the magnetic saturation, isolates the paramagnetic susceptibility, and the directional set therefore isolates the paramagnetic component of the bulk AMS. This paramagnetic component is carried primarily by the ferromagnesian silicates, in this case mainly biotite. The high-field AMS fabrics represent mostly the biotite magnetocrystalline subfabric. The fabric of mafic silicates in high-grade gneisses is acquired not only through crystal plastic deformation mechanisms in the melanosome (unmolten fraction of the migmatites) but also through rigid body particle rotation in the leucosome (molten fraction).

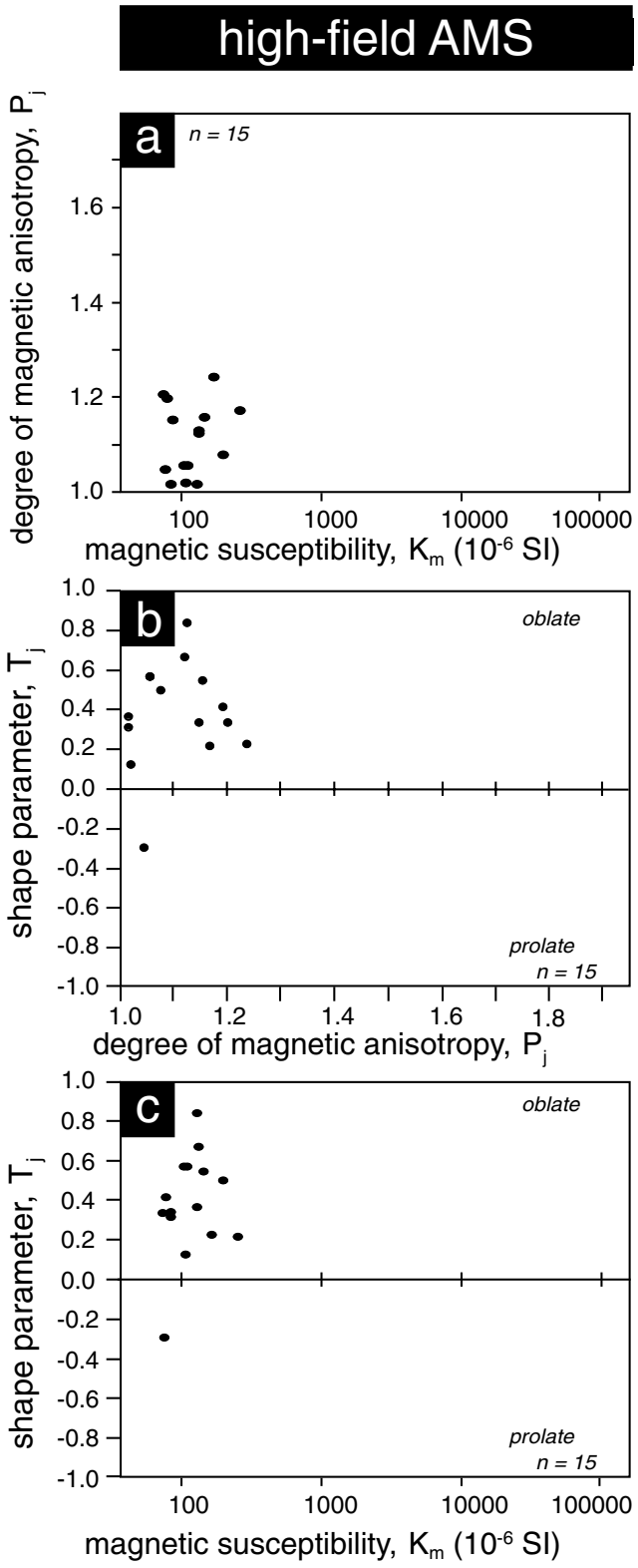

Figure 7. High-field AMS scalar results on oriented block Mo070.

It must be noted that the experimental procedure described here would yield incomplete separation of components if the specimens contained high-coercivity phases such as haematite. A solution to this problem is currently under development.

The torque results concern only the deviatoric (i.e. anisotropic) part of the magnetic fabric. Therefore the proportion of ferromagnetic to paramagnetic signal refers only to the magnetic anisotropy and not to the magnetic susceptibility. The principal directions of the torque ferromagnetism are similar to the low-field directions. The high-field AMS axes obtained using the VSM instrument and the low-field AMS axes obtained using the Kappabridge instrument significantly depart by about 13°. A comparison performed using the same 15 specimens for low-field and high-field AMS yields the same departure of 13°. This suggests that the magnetic fabric of magnetite is not coaxial with the magnetic fabric of biotite. A similar difference is observed between the torque magnetometer results and the low-field AMS results, interestingly with the same angle of departure. The similarity between the torque and the VSM results supports the existence of a significant angle of non-coaxiality between the paramagnetic AMS and the ferromagnetic AMS.

Furthermore, the ferromagnetic shape parameter obtained by torque magnetometry for specimen Mo070A1 is prolate ($U \approx -0.11$). The shape parameter obtained by low-field AMS for the same specimen is also prolate ($T \approx -0.13$). The paramagnetic shape parameter obtained by torque magnetometry for sample Mo070A1 is oblate ($U \approx 0.23$). The shape parameters obtained by high-field AMS for the same specimen are also oblate ($T \approx 0.38$; $U \approx 0.39$). This is in agreement with the fact that biotite has an intrinsically oblate magnetic ellipsoid (Ballet & Coey 1982; Beausoleil *et al.* 1983; Zapletal 1990; Martín-Hernández & Hirt 2003). The magnetic principal axes of the torque magnetometry fabric and that of the high-field AMS obtained with the VSM are essentially similar within instrumental error. The combined evidence provided by the torque magnetometer and the VSM instrument strongly suggests that the high-field magnetic fabrics actually represent the paramagnetic-only component to magnetic fabrics, i.e. in this case the subfabric of biotite. This hypothesis is strongly supported by the values obtained for the high-field degree of anisotropy of the purely paramagnetic fraction that never exceeds the value of 1.3 attributed to biotite single crystals (Zapletal 1990; Martín-Hernández & Hirt 2003).

6.3 Kinematic information and magnetic fabrics

Consistent structural asymmetries observed in the *XZ* section of the finite strain ellipsoid (Fig. 2) and differences in the orientation of the lineation for an amphibolite inclusion and its host (Ferré *et al.* 2003) suggest a significant non-coaxial component in the deformation of the studied migmatites. In addition, the consistent difference between the biotite subfabric (paramagnetic AMS) and the magnetite subfabric (ferromagnetic) further supports a non-coaxial strain.

The aspect ratios of biotite and magnetite grains are most probably different statistically, which may explain the non-parallelism of the subfabrics if deformation is non-coaxial (Fernandez *et al.* 1983). However, it is important to underline that at this stage we cannot quantify this aspect ratio or its spatial variability between the leucosome and the melanosome.

One of the most salient results of our investigations is that the shape parameter (T or U) depends to a large extent on the magnetic carrier (biotite or magnetite). This shows that the shape parameter should not be used as an absolute indication of the deformation regime even in cases where magnetic fabrics are controlled by only one mineral phase. The reliability of the magnetic anisotropy shape factor can also be marred by mixtures of intrinsically prolate and

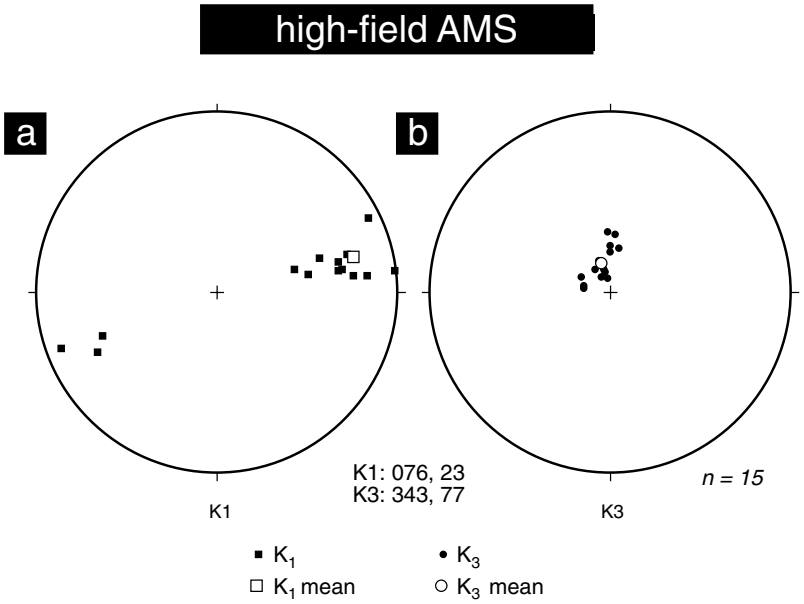

Figure 8. High-field AMS directional results on oriented block Mo070.

oblate markers or by mixtures of single-domain and multidomain magnetite grains (Ferré 2002).

7 CONCLUSION

Migmatites are lower crustal rocks that contain a wealth of information about deep flow processes. A better understanding of such processes may require us to split the rock fabric into its individual components. Magnetic fabric techniques have the potential to achieve this goal while keeping measurement times in perspective by using a combination of low- and high-field methods.

The high-field AMS method using a vibrating sample magnetometer has been modified to eliminate some of the sample shape effects and to reach higher saturation conditions by using smaller cubic specimens. This new method successfully isolates, in only 22 min per specimen, the paramagnetic susceptibility from a sample containing a mixture of ferromagnetic and paramagnetic carriers.

The principal axes of the magnetic fabrics faithfully represent the mean orientations of the magnetic carriers. However, the shape parameter (T or U) does not reflect the strain regime accurately because it is also strongly controlled by the intrinsic shape factor of the carriers.

In the studied material, a clear non-coaxiality has been unravelled between the paramagnetic AMS and the ferromagnetic AMS. This is attributed to a significant vorticity component in the regional deformation.

ACKNOWLEDGMENTS

Two anonymous reviewers are respectfully thanked for their constructive comments. The Gibson Fund (University of Minnesota) provided support for ECF during his sabbatical at the University of Minnesota. Access to the Morton quarries was kindly arranged with permission from Cold Springs Granite through Chuck Mulhbauer. Jim Thill, Emma Rainey and Jim Marvin provided tremendous help at the Institute for Rock Magnetism (IRM). The IRM is supported by the Instruments and Facilities Programme, Earth Sciences Division, NSF. ETH-Zurich is very sincerely thanked for making the torque magnetometer available to us.

REFERENCES

Ballet, O. & Coey, J.M.D., 1982. Magnetic properties of sheet silicates; 2:1 layer minerals, *Phys. Chem. Miner.,* **8,** 218–229.

Banerjee, S.K. & Stacey, F.D., 1967. The high-field torque-meter method of measuring magnetic anisotropy in rocks, in, *Methods in Palaeomagnetism*, pp. 470–476, eds Collinson, D.W., Creer, K.M. & Runcorn S.K., Elsevier, Amsterdam.

Bauer, R.L., 1974. Gneisses at Granite Falls and Montevideo, Minnesota. *MSc thesis* (unpublished), Missouri-Columbia.

Bauer, R.L., 1980. Multiphase deformation in the Granite Falls—Montevideo area, Minnesota River Valley, in, *Selected Studies of Archean Gneisses and Lower Proterozoic Rocks in the Southern Canadian Shield,*Geological Society of America Special Paper, pp. 1–17, ed. Hanson, G.N. & Morey, G.B, Geological Society of America, Boulder, CO.

Beausoleil, N., Lavallee, P., Yelon, A., Ballet, O. & Coey, J.M.D., 1983. Magnetic properties of biotite micas. *J. Appl. Phys.,* **54**, (2),906–915.

Bergmüller, F., Barlocher, C., Geyer, B., Grieder, Heller F., & Zweifel, P., 1994. A torque magnetometer for measurements of high-field anisotropy of rocks and crystals, *Meas. Sci. Technol.,* **5,** 1466–1470.

Borradaile, G.J. & Henry, B., 1997. Tectonic applications of the magnetic susceptibility and its anisotropy. *Earth Sci. Rev.,* **42,** 49–93.

Bouchez, J.L., 1997. Granite is never isotropic: an introduction to AMS studies of granitic rocks, in, *Granite: from Segregation of Melt to Emplacement Fabrics. Petrology and Structural Geology*, pp. 95–112, eds Bouchez, J.L., Hutton, D.H.W. & Stephens, W.E., Kluwer, Dordrecht.

Cañón-Tapia, E., Walker, G.P.L. & Herrero-Bervera, E., 1996. The internal structure of lava flows-insights from AMS measurements: I-Near-vent a'a, *J. Volcanol. Geothermal Res.,* **70,** 21–36.

Collinson, D.W., Creer, K.M. & Runcorn, S.K., 1967. *Methods in Paleomagnetism*, Elsevier, Amsterdam.

Day, R., Fuller, M. & Schmidt, V.A., 1977. Hysteresis properties of titanomagnetites: grain-size and compositional dependence, *Phys. Earth planet. Int.,* **13,** 260–267.

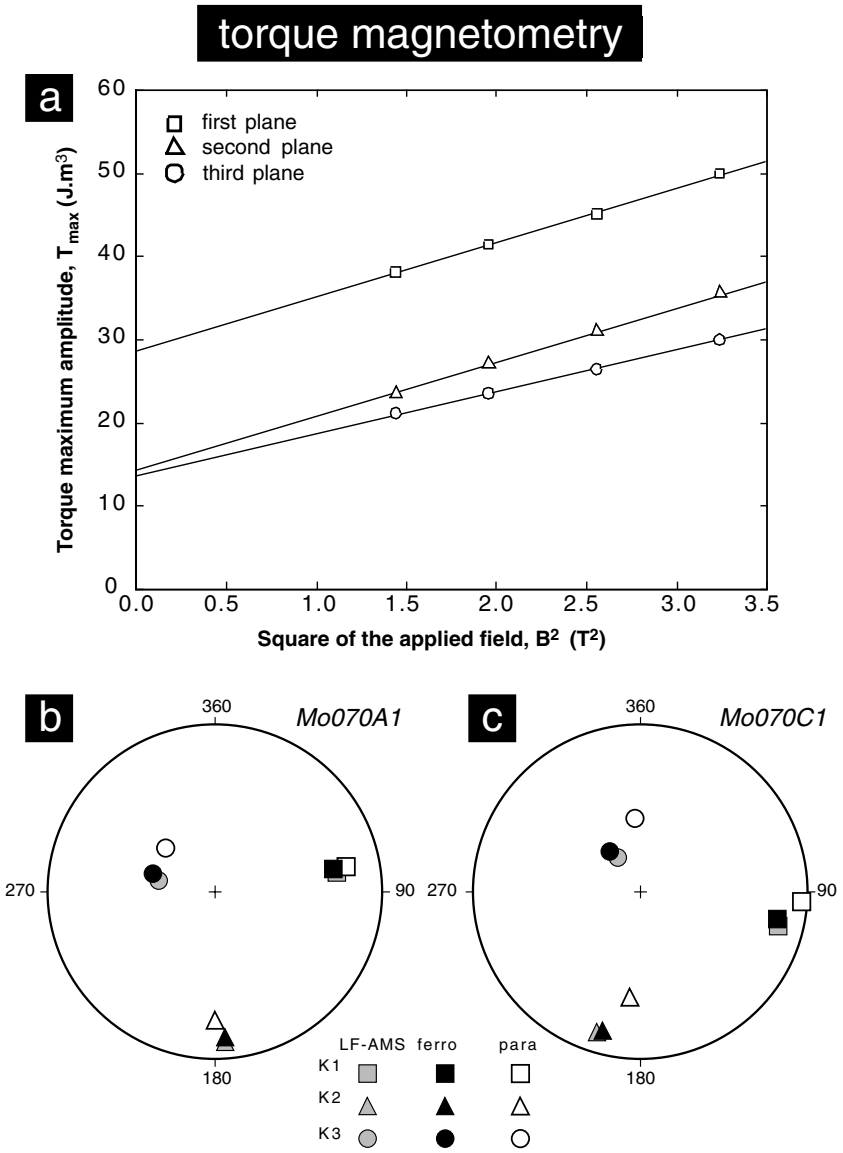

Figure 9. Torque magnetometry results on oriented block Mo070.

Fernandez, A., Feybesse, J.-L. & Mezure, J.-F., 1983. Theoretical and experimental study of fabrics developed by different shaped markers in two-dimensional simple shear. *Bull. Soc. geol. France,* **25,** 319–326.

Ferré, E.C., 2002. Theoretical models of intermediate and inverse ferromagnetic, low-field AMS fabrics. *Geophys. Res. Lett.,* **29**, 7, 10.1029/2001GL1436667.

Ferré, E.C., Thill, J.W., Rainey, E.S.G. & Teyssier, C., 2000. Ductile flow in migmatites deduced from combined low- and high-field AMS measurements, *EOS, Trans. Am. geophys. Un.,* **81**,(48), 367.

Ferré, E.C., Teyssier, C., Jackson, J., Thill, J.V. & Rainey, E.S.G., 2003. Magnetic susceptibility anisotropy: a new petrofabric tool in migmatites, *J. geophys. Res.,* **108,** doi:10.1029/2002JB001790.

Goldich, S.S., Wooden, J.L., Ankenbauer, G.A.J., Levy, T.M. & Suda, R.U., 1980. *Origin of the Morton Gneiss, Southwestern Minnesota: Part 1, Lithology,*Geological Society of America Special Paper 182, pp. 45–56.

Henry, B., 1983. Interprétation quantitative de l'anisotropie de susceptibilité magnétique, *Tectonophysics,* **91,** 165–177.

Hopgood, A.M., 1998. *Determination of Structural Successions in Migmatites and Gneisses*, Kluwer Academic, Dordrecht.

Hrouda, F., 1982. Magnetic anisotropy of rocks and its application in geology and geophysics, *Geophys. Surv.,* **5,** 37–82.

Hrouda, F., 2002. The use of the anisotropy of magnetic remanence in the resolution of the anisotropy of magnetic susceptibility into its ferromagnetic and paramagnetic components, *Tectonophysics,* **347,** 269–281.

Hrouda, F. & Jelinek, F., 1985. Resolution of ferromagnetic and paramagnetic anisotropy components, using low-field and high-field measurements, *Assembly of the International Association of Geomagnetism and Aeronomy, IAGA, Prague*, 5–7 August, p. 206. IAGA, Praha.

Hrouda, F. & Jelinek, V., 1990. Resolution of ferrimagnetic and paramagnetic anisotropies in rocks, using combined low-field and high-field measurement, *Geophys. J. Int.,* **103,** 75–84.

Jackson, M., 1991. Anisotropy of magnetic remanence: a brief review of mineralogical sources, physical origins and geological applications, *Pure appl. Geophys.,* **136,** 1–28.

Jelínek, V., 1977. *The Statistical Theory of Measuring Anisotropy of Magnetic Susceptibility of Rocks and its Applications*, 88 pp, Geofysika, Brno.

Jelínek, V., 1978. Statistical processing of anisotropy of magnetic susceptibility measured on groups of specimen, *Stud. Geofyz. Geodet.,* **22,** 50–62.

Jelínek, V., 1981. Characterization of the magnetic fabrics of rocks, *Tectonophysics,* **79,** T63–T67.

Jelínek, V., 1993. Theory and measurement of the anisotropy of isothermal remanent magnetization of rocks, *Trav. Géophys.,* **37**, 124–134.

Kelso, P., Tikoff, B., Jackson, M. & Sun, W., 2002. A new method for the separation of paramagnetic and ferromagnetic susceptibility anisotropy using low field and high field methods, *Geophys. J. Int.,* **151,** 345–359.

Martín-Hernández, F. & Hirt, A.M., 2001. Separation of ferrimagnetic and paramagnetic anisotropies using a high-field torsion magnetometer, *Tectonophysics,* **337,** 209–221.

Martín-Hernández, F. & Hirt, A.M., 2003. Paramagnetic anisotropy of magnetic susceptibility in biotite, muscovite and chlorite single crystals, *Tectonophysics,* **367,** 13–28.

McLellan, E.L., 1983. Problems of structural analysis in migmatite terrains, in, *Migmatites, Melting and Metamorphism*, pp. 299–302, eds Atherton, M.P. & Gribble, C.D., Shiva Publishing, Nantwich.

Nielsen, B.V. & Weiblen, P.W., 1980. *Mineral and Rock Compositions of Mafic Enclaves in the Morton Gneiss*, Geological Society of America Special Paper 182, 95–103.

Noltimier, H.C., 1971. Determining magnetic anisotropy of rocks with a spinner magnetometer giving in-phase and quadrature data output, *J. geophys. Res.,* **76,** 4849–4854.

Parès, J.M. & van der Pluijm, B.A., 2003. Room- and low-temperature magnetic anisotropy and tectonic strain in weakly deformed mudrocks, *Geophys. Res. Abs.,* **5,** 04238.

Passchier, C.W., Myers, J.S. & Kröner, A., 1990. *Field Geology of High-grade Gneiss Terrains*, Springer, Berlin.

Porath, H. & Chamalaun, F.H., 1966. The magnetic anisotropy of hematite bearing rocks, *Pure appl. Geophys.,* **67,** 81–88.

Richter, C., van der Pluijm, B.A. & Housen, B.A., 1993. The quantification of crystallographic preferred orientation using magnetic anisotropy, *J. Struct. Geol.,* **15,** 113–116.

Rochette, P. & Fillion, G., 1988. Identification of multicomponent anisotropies in rocks using various field and temperature values in a cryogenic magnetometer, *Phys. Earth planet. Int.,* **51,** 379–386.

Rochette, P., Jackson, M. & Aubourg, C., 1992. Rock magnetism and the interpretation of anisotropy of magnetic susceptibility, *Rev. Geophys.,* **30,** 209–226.

Southwick, D.L. & Chandler, V.W., 1996. Block and shear-zone architecture of the Minnesota River valley subprovince: implications for late Archean accretionary tectonics, *Can. J. Earth Sci.,* **33,** 831–847.

Tarling, D.H. & Hrouda, F., 1993. *The Magnetic Anisotropy of Rocks*, Chapman & Hall, London.

Thill, J.W., Ferré, E.C., Rainey, E.S.G. & Teyssier, C., 2000. Separation of AMS into ferrimagnetic and paramagnetic components in migmatites: a possible shear-sense indicator? *EOS, Trans. Am. Geophys. Un.,* **81**, (48), 367.

Vigneresse, J.L., Barbey, P. & Cuney, M., 1996. Rheological transitions during partial melting and crystallization with application to felsic magma segregation and transfer, *J. Petrol.,* **37,** 1579–1600.

Zapletal, K., 1990. Low-field susceptibility anisotropy of some biotite crystals, *Phys. Earth planet. Int.,* **63,** 85–97.

Zen, E., 1988. Thermal modelling of stepwise anatexis in a thrust-thickened sialic crust, *Trans. R. Soc. Edinb.,* **79,** 223–235.